Journal of the European Ceramic Society 21 (2001) 2393–2405

www.elsevier.com/locate/jeurceramsoc

Influence of additives on corrosion resistance and corroded microstructures of MgO–C refractories

S. Zhang, W.E. Lee *

Department of Engineering Materials, The University of Sheffield, Sheffield S1 3JD, UK

Received 6 October 2000; received in revised form 11 December 2000; accepted 16 December 2000

Abstract

Corrosion resistance and corroded microstructures of MgO–C refractories containing various antioxidants in a model EAF slag (CaO/SiO_2 weight ratio = 1.38) were investigated after 30 h at 1650°C. Antioxidants influenced their corrosion resistance by affecting both carbon (C) oxidation and MgO dissolution in the slag. Al additions improved C oxidation resistance at 1650°C only a little, but accelerated MgO dissolution, resulting in a minor effect on corrosion resistance. Additions of Si or Al + Si improved C oxidation resistance slightly but accelerated MgO dissolution more than Al additions, resulting in worse corrosion resistance than Al addition and no addition. B_4C conferred the worst corrosion resistance, since boron-containing liquid formed in the refractory, greatly accelerating MgO dissolution and resulting in C (mainly graphite) in the matrix being eroded easily by the slag. With double addition of Al + B_4C, boron-containing liquid formed, which not only inhibited effectively C (mainly graphite) oxidation, but also accelerated formation and growth of $MgAl_2O_4$ spinel (MA) crystals between graphite in the matrix at the test temperature. In this case, even though MgO dissolution was accelerated to some extent, graphite was not easily washed away by the slag because it was effectively protected from oxidation and held in place by MA crystals. This maintained the integrity of the refractory texture, giving the Al + B_4C containing refractory the best corrosion resistance.

Keywords: Antioxidants; Carbon; Corrosion; MgO; Microstructure-final; Refractories

1. Introduction

The presence of carbon (C) in MgO–C refractories confers many desirable properties such as excellent thermal shock and corrosion resistance. However, it is highly vulnerable to oxidation and induces low mechanical strength due to its weakly-bonded nature. To overcome these drawbacks, so-called antioxidants are usually added to the refractory batches during brick fabrication.

Antioxidants often used in MgO–C refractories include metals/alloys (such as aluminium, silicon and Al/Mg alloys), carbides (such as B_4C and SiC), and boron-based compounds (such as CaB_6 and ZrB_2).[1–5] These antioxidants function in different ways during the refractories use. Metal/alloy and carbide additives mainly act as CO-reducing agents, contributing to carbon oxidation inhibition and/or improvement in hot strength by forming high-temperature ceramic bonds. Boron-based additives, on the other hand, act to block open pores to reduce the carbon oxidation by forming liquid phases.

The antioxidants are also known to affect the corrosion resistance of MgO–C refractories. SiC has been used to improve the corrosion resistance and it has been additionally observed to retard carbon oxidation although the mechanism has not been specified. When the SiC content is below ~5 wt.%, wear rate of the bricks decreases with increasing SiC content, but above ~5 wt.%, owing to excessive formation of SiO_2, the corrosion resistance begins to decrease.[6] Conversely, Nagai et al.[7] indicated that addition of SiC always decreases corrosion resistance of MgO–C refractories. Naefe et al.[8] reported that addition of Al or Mg improves, and Si decreases, the corrosion resistance, whereas Morimoto et al.[9] found that addition of these antioxidants had no obvious effect on corrosion resistance. Contrarily, Baker and Brezny[10] determined that metal additions (Al, Si and Mg) encouraged severe corrosion in all MgO–C refractories at the 5 wt.% metal level. Clearly, whether addition of antioxidants (in particular Al) is beneficial or harmful is still a subject of controversy. Although the disagreement

* Corresponding author. Tel.: +44-114-2225474; fax: +44-114-222 5943.

E-mail address: w.e.lee@sheffield.ac.uk (W.E. Lee).

0955-2219/01/$ - see front matter
PII: S0955-2219(01)00208-4

has been attributed to refractories factors such as graphite purity,[11] MgO quality,[12] and MgO–C reaction,[10] a recent analysis by the present authors[13] reveals that slag composition (in particular, basicity) may play an important role. Al additions have a positive effect on corrosion resistance in a basic slag but little effect in an acid slag.[13]

Besides additions of single antioxidants, simultaneous additions of two antioxidants such as Al + Si[14] and Al + CaB_6[5] (termed here double addition) have also been introduced. The benefit of this type of addition is that it inhibits carbon oxidation more effectively than a single antioxidant[5,14,15] and in some specific cases such as double addition of Al + CaB_6 contributes to the improved corrosion resistance,[5,15] although the mechanism has not been specified.

In spite of these studies, the influence of additives (especially in the case of double addition) on corrosion mechanisms and corroded microstructures of MgO–C refractories is not yet clearly understood. This will be addressed in the present paper by measuring relative corrosion rates with a rotary slag test, examining corroded microstructures, and relating these to thermodynamic predictions.

2. Experimental and calculation procedures

2.1. Refractories and slag fabrication

Commercial Australian fused magnesia (40 wt.%), sintered magnesia (40 wt.%), and Chinese graphite flake (20 wt.%) with chemical compositions shown in Table 1 comprised the basic refractories mix. The following additives (provided by Baker Refractories Co., Worksop, UK), 5 wt.% aluminium (Al), 5 wt.% silicon (Si), 5 wt.% B_4C, 2.5 wt.% Al + 2.5 wt.% Si, and 2.5 wt.% Al + 2.5 wt.% B_4C were made individually. Phenolic resin 3 wt.% (Borden Ltd. Southampton, UK) was used as a binder. Applied pressure for shaping (uniaxial press) the six bricks was 270 MPa. After pressing, the bricks were cured at 270°C for 1 h. The apparent porosities and bulk densities of the bricks were almost identical, being ~4 vol.% and ~2.8 g/cm^3 respectively.

A model EAF slag with a chemical composition shown in Table 2 was synthesised from the starting powders comprising reagent grade $CaCO_3$ and $MgCO_3$ (BDH Laboratory Supplies, Poole, UK), Fe_2O_3, Al_2O_3 and MnO (Aldrich Chemical Co., Inc., Gillingham, UK) and Loch Aline silica sand (SiO_2; Tilcon, Stoke, UK). The synthesis process of the slag was reported previously.[16]

Table 1
Chemical composition of basic raw materials (wt.%)

	MgO	C	SiO_2	Al_2O_3	Fe_2O_3	CaO	Mn_3O_4	B_2O_3
Fused magnesia	97.55	–	0.37	0.03	0.06	1.86	0.11	0.004
Sintered magnesia	96.88	–	0.48	0.06	0.14	2.20	0.14	0.008
Graphite flakes	0.13	96.80	1.50	0.55	0.73	0.15	–	–

Table 2
Chemical composition of model slag (wt.%)

SiO_2	Al_2O_3	Fe_2O_3	CaO	MgO	MnO	CaO/SiO_2
23.5	12.5	17.5	32.4	5.4	8.9	1.38

2.2. Corrosion testing and microstructural characterisation

A conventional rotary slag test was used to compare the refractories relative corrosion rates. An advantage of this test is that it includes the effects of both corrosion and some erosion.[17] All tests were conducted at 1650°C for 30 h. The liquid slag was removed every 30 min and replaced with 300 g of fresh powdered slag to ensure constant slag composition during the test. Propane (C_3H_8) and pure oxygen (O_2) were used as the fuel. Particular attention was paid to avoiding temperature fluctuation during the test by adjusting the burning fuel valves. The temperature inside the rotary drum was checked every 10 min using a pyrometer.

After the corrosion test, the furnace was allowed to cool to room temperature and relative corrosion rates (corrosion index) were calibrated by taking the corrosion depth of the additive-free refractory as 100. The corroded samples were sectioned perpendicular to the refractory/slag interface and mounted in cold setting resin. Standard ceramographic grinding and polishing techniques then were used, after which all samples were carbon-coated and examined by backscattered electron imaging (BEI) and secondary electron imaging (SEI) in a Camscan Series 2A SEM or in some cases in a Jeol 6400 using its windowless energy dispersive spectroscopy (EDS) detector. EDS analysis was performed in the SEM using a LINK detector and AN10000 package. XRD (Philips powder diffractometer 1710 with Ni filtered CuK_α radiation) was also conducted to assist identification of the phases formed in the microstructures.

2.3. Thermodynamic calculations

Equilibrium thermodynamic calculations were performed with the DOS version 2.00 of FACT (Facility for Analysis of Chemical Thermodynamics) package.[18] The Gibbs energy minimization module EQUILIBRIUM was used together with the FACT databases. CO (10g) and O_2 (10g) were included in the system to model the atmosphere surrounding the samples. The effect

of slag attack was modelled by successive additions of slag to the refractories systems monitored by the parameter Alpha, i.e. the weight ratio of slag to refractory. When Alpha = 7 the calculation was carried out with 700 g of slag and 100 g of the refractory. The changes in predicted phase constitutions with Alpha were examined, and the results were plotted as log mole of phase versus Alpha.

3. Results

3.1. Thermodynamic predictions

Fig. 1 shows predicted major phase changes of the additive-free MgO–C refractory with Alpha. Upon increasing Alpha, C and MgO contents decrease, whereas unsurprisingly slag phase content increases. C and MgO contents drop abruptly to zero when Alpha reaches ~2.2 and ~6.0, respectively. Liquid Fe and Mn metals are also predicted and the content of the former is higher than that of the latter at the same Alpha. The main gaseous phases predicted include CO(g), CO_2(g), Mg(g), Fe(g) and Mn(g). Although varying with Alpha, their partial pressures are all higher than 10^{-5} atm. Predicted chemical composition (not shown), of the slag phase shown in Fig. 1, indicates that before MgO disappears (i.e. Alpha < ~6.0), the relative MgO content in the slag phase increases with increasing Alpha, whereas FeO and MnO contents decrease.

Predicted major phase changes of the Al added refractory with Alpha are given in Fig. 2. Formation of $MgAl_2O_4$ spinel (MA) is predicted, although its content drops to zero when it reacts with only a small amount of slag (Alpha≈0.05). Other predicted phases are the same as those predicted for the additive-free refractory (Fig. 1), however, in this case, C disappears at a higher Alpha value (~3.0) and MgO at a lower value (~5.8).

Calculations on the effect of other additions to the basic refractory mix reveal that the interaction between the slag and refractories results in similar patterns of predicted phase changes. Significant differences include (1) for Si addition, Mg_2SiO_4 forsterite (M_2S) is predicted, although its content drops to zero when it reacts with only a small amount of slag (Alpha~0.05), and (2) depending on the additive type, the Alpha value at which C and MgO disappear varies. For comparison, the C and MgO content changes with Alpha for all additions are presented together in Fig. 3. Alpha corresponding to C disappearance increases in the following order: additive-free (~2.2) < Al (~3.0) < Al + Si≈Si (~3.2) < Al + B_4C (~3.4) < B_4C(~3.6). However, Alpha corresponding to MgO disappearance has the reverse order: B_4C(~4.8) < Al + B_4C (~5.4) < Al + Si≈Si (~5.6) < Al (~5.8) < additive-free (~6.0).

3.2. Corrosion rates of MgO–C refractories

Fig. 4 illustrates the relative corrosion rates (corrosion index) of the refractories. Compared to the additive-free refractory, the corrosion rate increased by ~26% with addition of Al + Si, by ~35% with addition of Si, and by ~97% with addition of B_4C. Corrosion was only slightly decreased (by ~3%) by addition of Al, but markedly decreased (by ~30%) by addition of Al + B_4C.

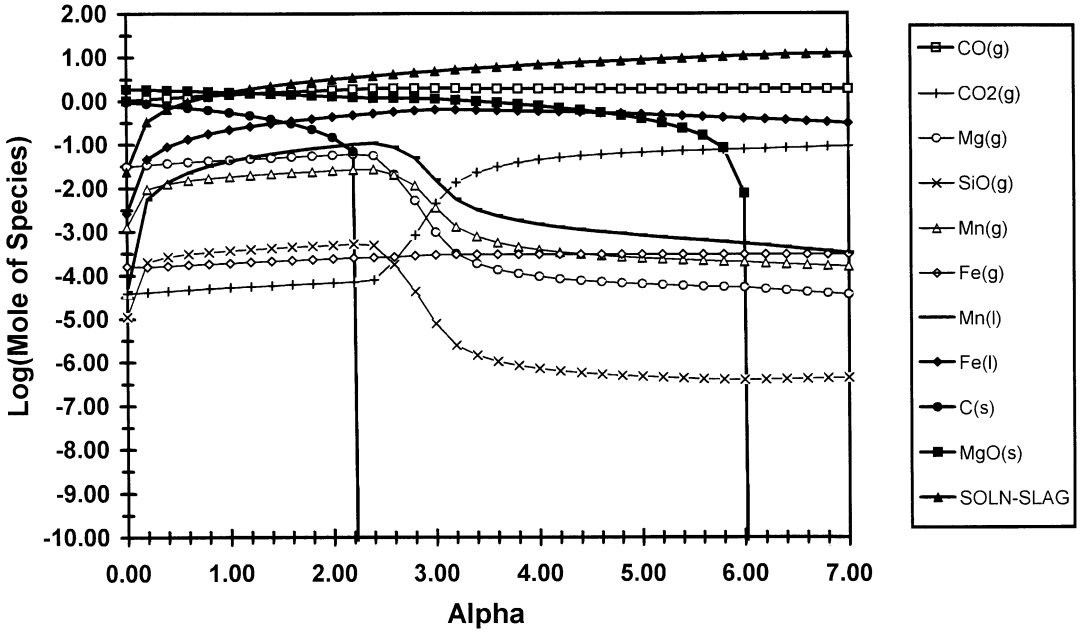

Fig. 1. Predicted major phase changes of additive-free MgO–C refractory with slag/refractory weight ratio (Alpha).

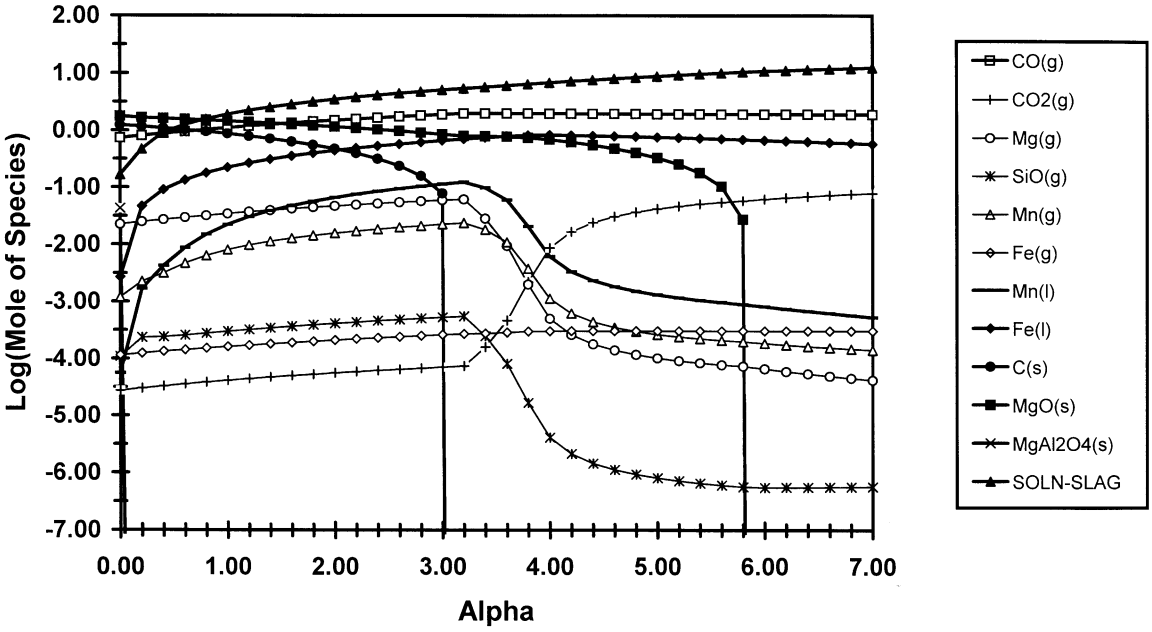

Fig. 2. Predicted major phase changes of Al added MgO–C refractory with slag/refractory weight ratio (Alpha).

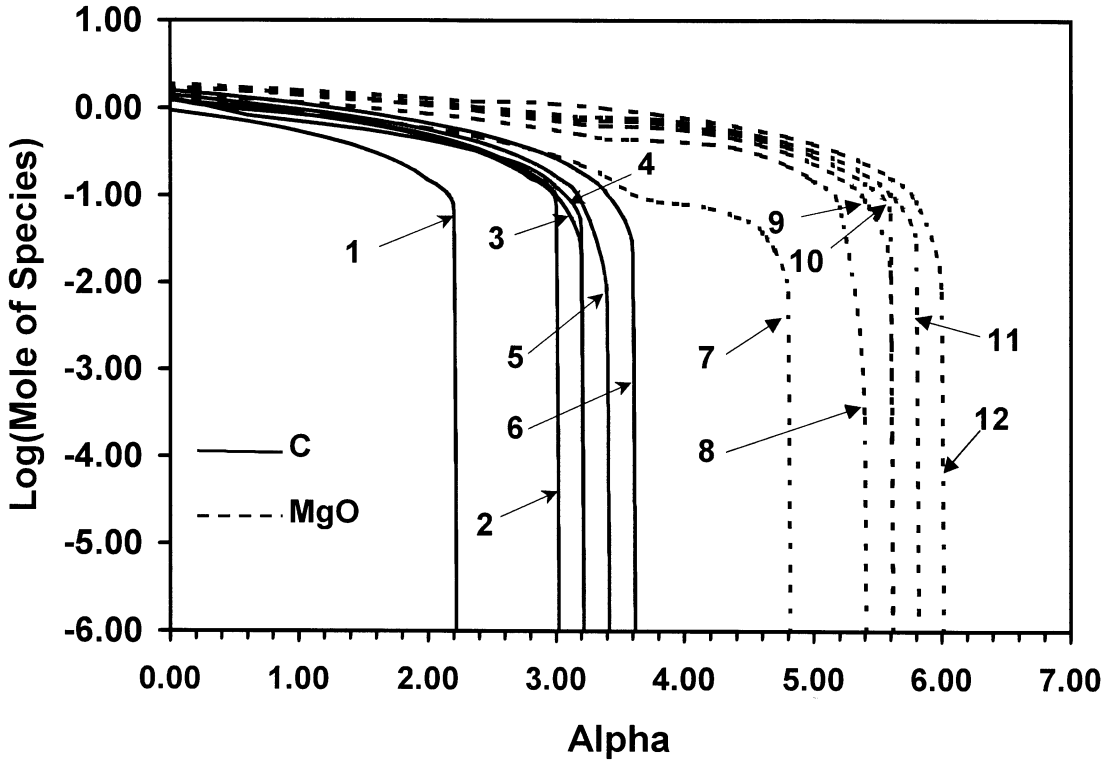

Fig. 3. Predicted MgO and C content changes in refractories containing various antioxidants with slag/refractory weight ratio (Alpha). 1 and 12: Additive-free; 2 and 11: Al addition; 3 and 10: Al + Si addition; 4 and 9: Si addition; 5 and 8: Al + B_4C addition; 6 and 7: B_4C addition.

3.3. Microstructures

3.3.1. As-cured microstructures

Microstructures of the MgO–C refractories after curing for 1 h at 270°C (not shown) revealed that large MgO angular grains (> 300 μm) were surrounded by a matrix comprising mainly graphite flakes, fine (< 50 μm) MgO, and the antioxidants (20–80 μm in size). EDS revealed that dicalcium silicate $CaO.2SiO_2$ (C_2S) was occasionally present at grain boundaries within

MgO aggregates, and an iron-containing silicate phase was present between graphite flakes. These impurity phases were believed to be from the original MgO and graphite raw materials (see Table 1).

3.3.2. Corroded microstructures

The corroded microstructure (BEI) of the additive-free refractory (Fig. 5) reveals an uncorroded layer on the left hand side, whose microstructure was similar to the as-cured microstructure. Adjacent to this uncorroded layer was a thin (~900 μm) layer in which slight slag penetration was observed. Higher magnification (not shown) revealed some decarburisation in this slag penetrated layer. Next to the slag penetrated layer was a ~3400 μm thick decarburised layer in which no graphite was present and many large angular voids (>1000 μm) and some smaller rounded pores (10–30 μm) were observed. The remaining MgO aggregates were covered and some of them disintegrated by slag (light grey contrast) which, EDS revealed, comprised mainly CaO, MgO, SiO_2 and Al_2O_3. A few rounded phases (white contrast) were also found in this layer. EDS confirmed that they were Fe metal containing a small amount of Mn. Next to the decarburised layer was a denser layer

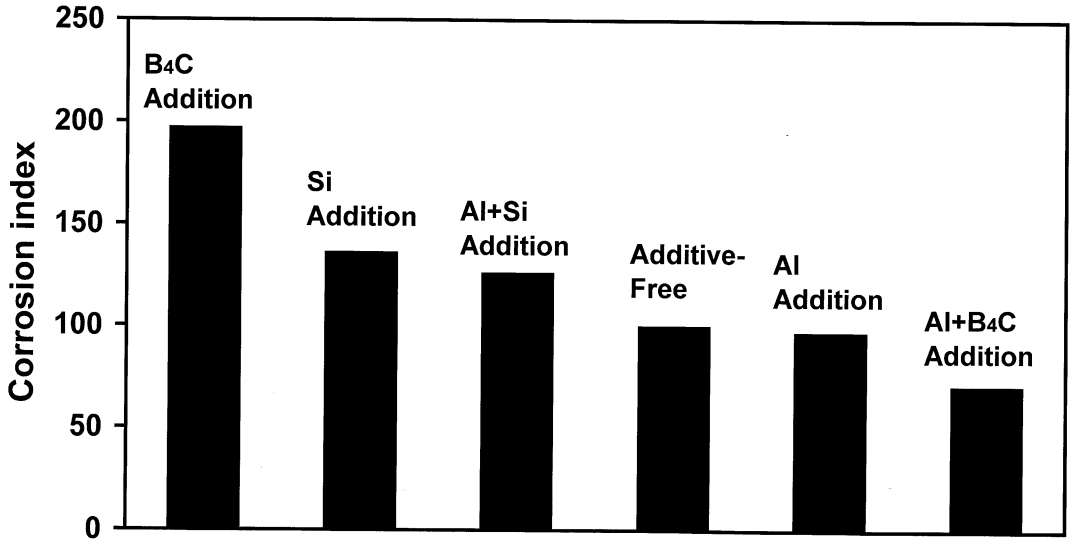

Fig. 4. Relative corrosion rates of MgO–C refractories containing various antioxidants.

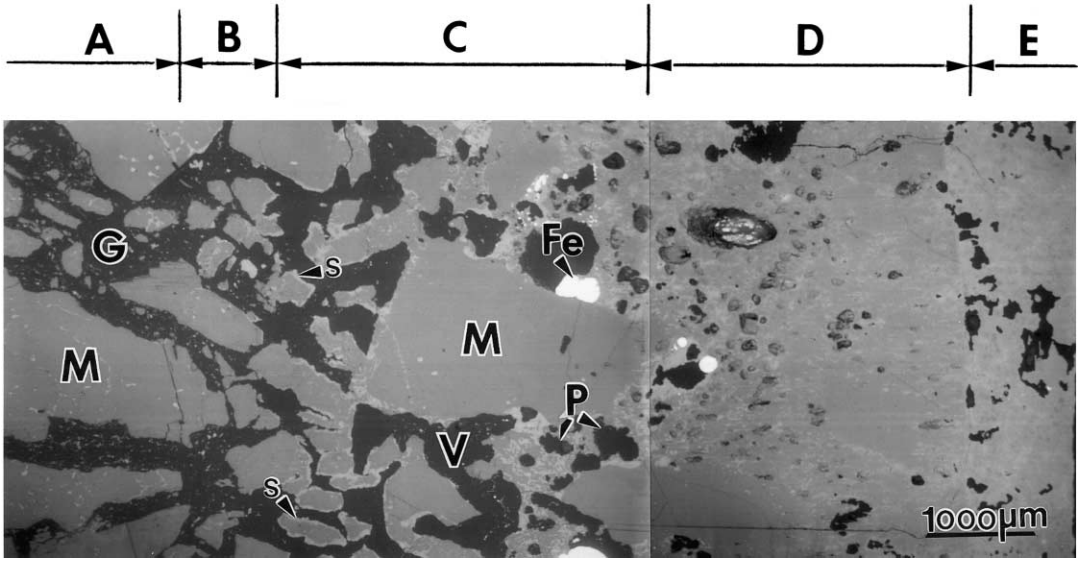

Fig. 5. Corroded microstructure (BEI) of additive-free refractory. Slag penetrated, decarburised and dense MgO layers were observed between uncorroded refractory and slag layers. No carbon was present in the decarburised layer and Fe + minor Mn (white contrast) was found. MgO grains in the decarburised layer were corroded and some disintegrated by the slag. Slag was present in the dense MgO layer although it is seen more clearly in Fig. 6. M = MgO, V = void, P = pore, G = graphite, S = slag. A: uncorroded layer; B: slag penetrated layer; C: decarburised layer; D: dense MgO layer; E: slag layer.

(~2950 μm) which at higher magnification (Fig. 6) was revealed to comprise mainly MgO and some slag phase and a few pores (the layer is termed here the dense MgO layer). Beyond the dense MgO layer was the remnant slag layer. Higher magnification (not shown) of the remnant slag layer, along with EDS and XRD, confirmed that the slag contained small amounts of angular C_2S, angular complex spinel [[Fe,Mn,Mg]O.$(Fe,Al)_2O_3$], and lath-shaped melilite (a solid solution between gehlnite C_2AS, and akermanite, C_2MS_2). Besides these phases, some rounded MgO grains (~50μm) were also found in the slag close to the dense MgO layer. EDS revealed that these MgO grains were covered by merwinite, C_3MS_2, shells and inside of them some FeO and MnO had precipitated.

The corroded microstructure of the Al added refractory (Fig. 7) is similar to that of the additive-free refractory (Fig. 5), containing five different layers, i.e. uncorroded, slag penetrated, decarburised, dense MgO and remnant slag layers. MA crystals (1–2 μm) were identified in the uncorroded refractory layer (Fig. 8) and the slag penetrated layer (not shown) by EDS along with XRD. In the slag penetrated layer, some MgO grains were corroded by the penetrating slag and some decarburisation was observed. Compared with that shown in Fig. 5, a slightly thinner (~3150 μm) decarburised layer was found, in which, MgO grains were disintegrated and corroded by the slag and massive >1000 μm voids were also observed. The MgO dense layer (~2850 μm) was a little thinner than that shown in Fig. 5, and EDS revealed that more Al_2O_3-rich silicate slag was present in the dense MgO layer and more MgO grains in the layer were corroded.

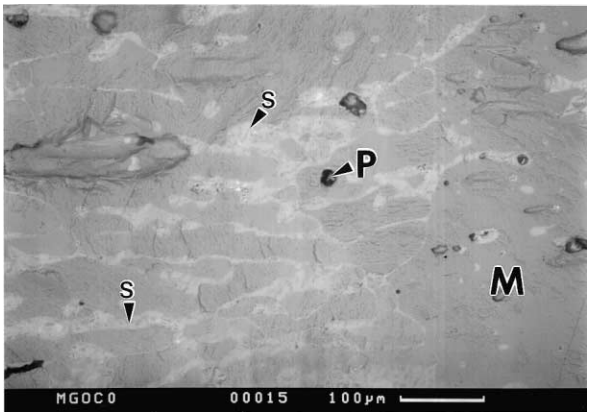

Fig. 6. Higher magnification BEI of the dense MgO layer shown in Fig. 5, revealing silicate slag (S) and a few pores (P).

The same five layers were also observed in the corroded microstructure of the Si added refractory (Fig. 9). The decarburised layer (~3100 μm) was slightly thinner than that in both additive-free (Fig. 5) and Al added refractories (Fig. 7), but the dense MgO layer (~1950 μm) became much thinner. Slag penetration into the dense MgO and the decarburised layers was also evident. No M_2S was detected in the MgO dense layer, but it was identified by EDS and XRD in the uncorroded and slag penetrated layers.

The macrostructure of the Al + Si added refractory after corrosion (not shown) was similar to that of the Si added refractory shown in Fig. 9. One difference was that a little thicker (~2100 μm) dense MgO layer formed and in the uncorroded layer, MA (1–2 μm) and many SiC crystals (20–50 μm) were identified by EDS along with XRD.

The corroded microstructure of the B_4C added refractory (Fig. 10) was different from those of the other four refractories. Between the slag penetrated and slag layers only a porous layer (termed here the corroded layer), which contained massive pores (>1000 μm) and

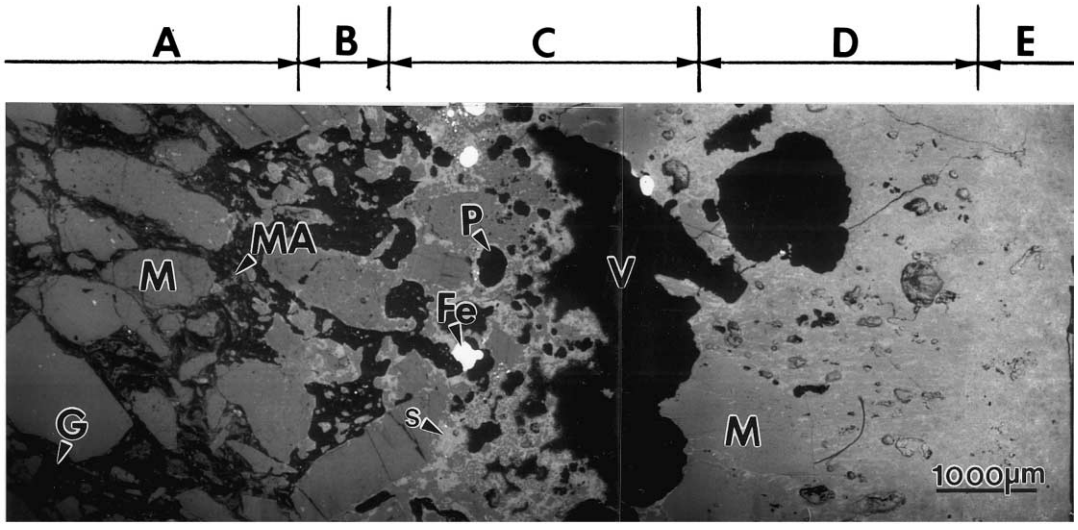

Fig. 7. Corroded microstructure (BEI) of Al added refractory. The dense MgO and decarburised layers were penetrated and corroded by the slag. $MgAl_2O_4$ spinel (MA) was found in the uncorroded layer, although its morphology is seen more clearly in Fig. 8. M = MgO, V = void, P = pore, G = graphite, S = slag. A: uncorroded layer; B: slag penetrated layer; C: decarburised layer; D: dense MgO layer; E: slag layer.

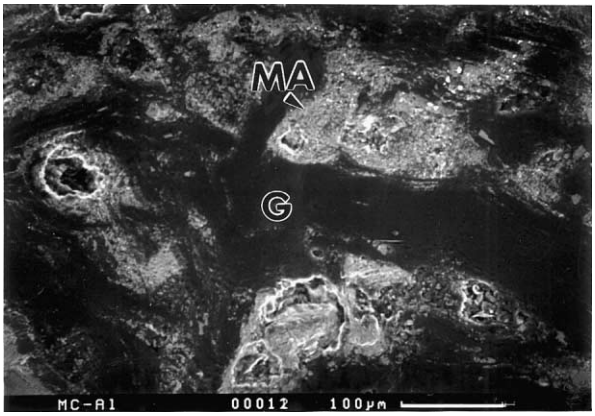

Fig. 8. High magnification BEI of the matrix in the uncorroded layer shown in Fig. 7. Large amounts of $MgAl_2O_4$ spinel (MA) were found between graphite (G).

a few severely corroded MgO grains, was observed. In the slag penetrated layer some MgO grains were corroded. Large amounts of lath-shaped M_3B phases were identified in the uncorroded layer by EDS along with XRD (not shown).

The corroded microstructure of the refractory with $Al + B_4C$ addition (Fig. 11), reveals a thin (1500–2500 μm) dense MgO layer containing high levels of slag adjacent to the remnant slag layer. Nevertheless, between the MgO dense layer and the uncorroded layer only thin (< 1000 μm) slag penetrated and decarburised layers were present. No obvious decarburisation was observed in the slag penetrated layer. Higher magnification of the uncorroded (Fig. 12) and penetrated layers (not shown) revealed that angular or lath-shaped dark grey contrast phases and angular light contrast phases were present between the graphite flakes. EDS along with XRD confirmed that the dark grey contrast phases were M_3B whereas the light contrast phases coexisting with the M_3B were MA crystals (with average size: ~10 μm).

4. Discussion

4.1. Corrosion mechanism and corroded microstructure of basic MgO–C refractory

Thermodynamic calculations (Fig. 1) indicate that continuous interaction between the slag and the refractory (increasing Alpha), leads to the loss of two main refractory components, C and MgO. The predicted slag composition reveals no obvious solubility of C in the slag, suggesting that the C loss is not likely to be due to its dissolution in the slag. As shown in Fig. 1, after the interaction between the slag and the refractory, gaseous phases such as CO(g) and CO_2(g), and metals such as Fe and Mn form and, at the same time, the partial pressure of O_2 originally from the atmosphere becomes very low ($< 10^{-7}$ atm). These suggest that the C loss is mainly due to its oxidation by the O_2 from the atmosphere and/or by the oxidising components such as Fe_xO and MnO from the slag, which can be indicated by the following reactions.

$$2C(s) + O_2(g) = 2CO(g) \quad (1)$$

$$C(s) + O_2(g) = CO_2(g) \quad (2)$$

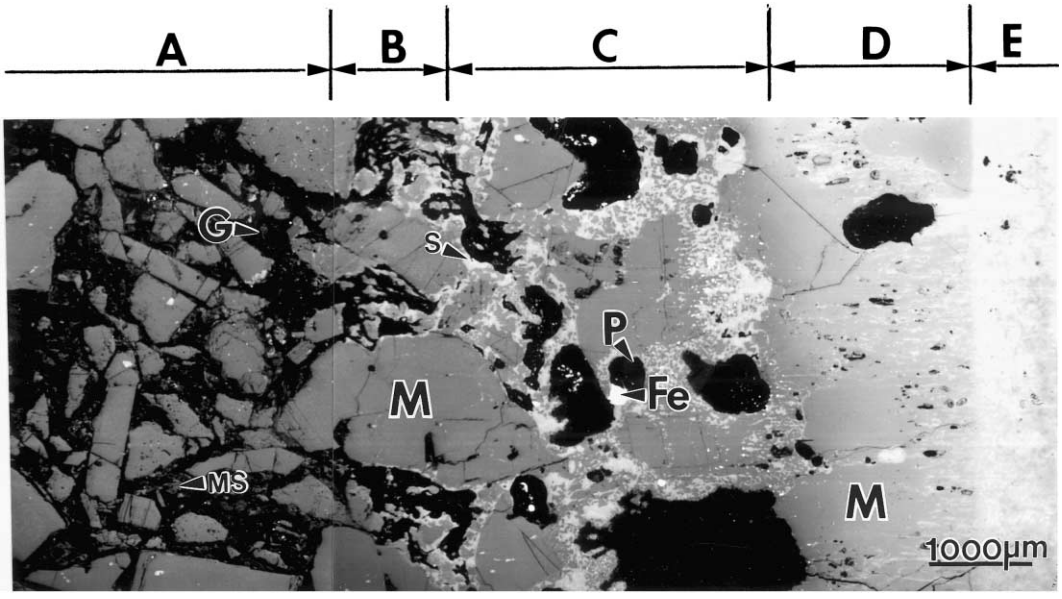

Fig. 9. Corroded microstructure (BEI) of Si added refractory. A thin dense MgO layer was observed. Slag penetration through the dense MgO and decarburised layers was evident. Mg_2SiO_4 forsterite was found in the uncorroded layer. M = MgO, P = pore, G = graphite, S = slag. MS = Mg_2SiO_4. A: uncorroded layer; B: slag penetrated layer; C: decarburised layer; D: dense MgO layer; E: slag layer.

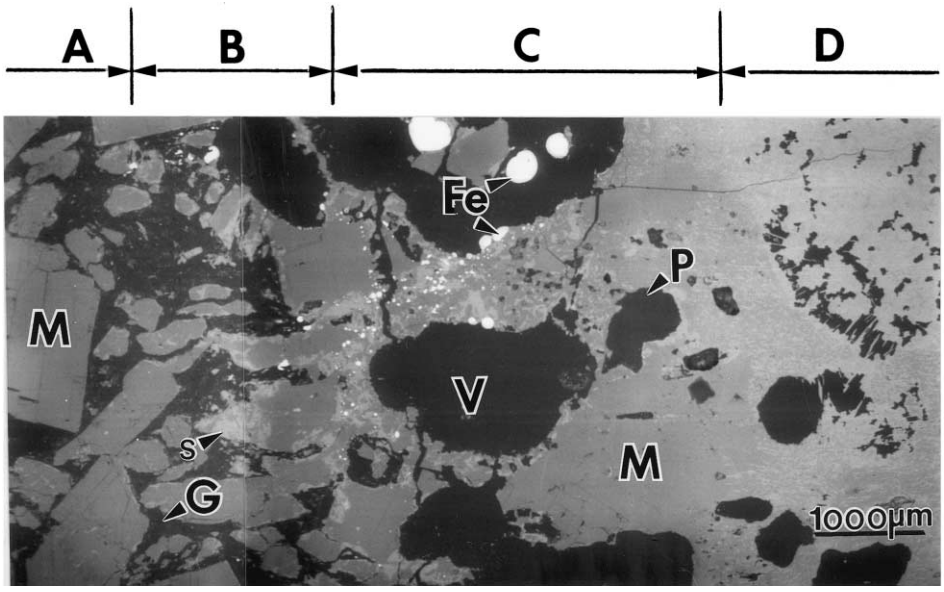

Fig. 10. Corroded microstructure (BEI) of B_4C added refractory. Between the slag penetrated and slag layers, a severely corroded porous layer was observed. Disintegration and corrosion of MgO by the slag was evident. M = MgO, V = void, P = pore, G = graphite, S = slag. A: uncorroded layer; B: slag penetrated layer; C: corroded layer; D: slag layer.

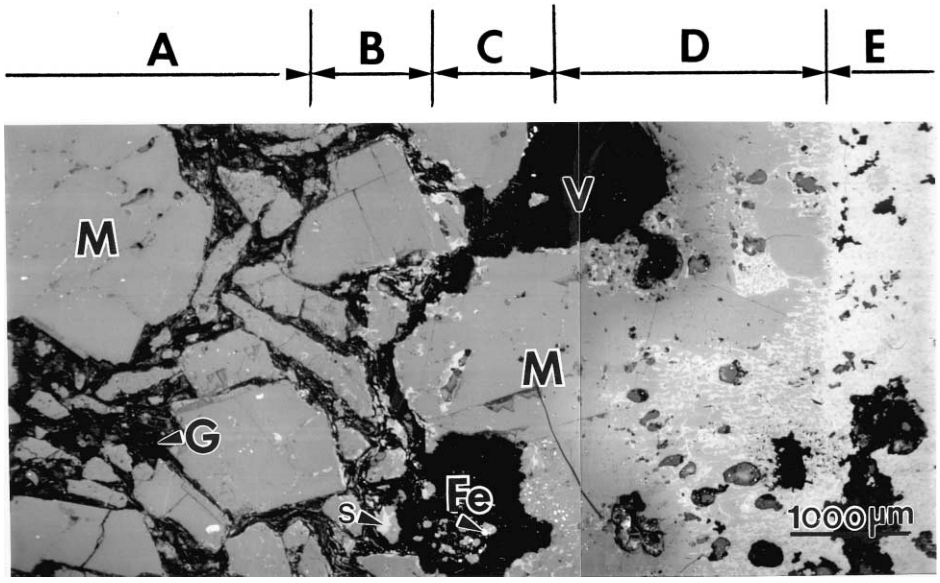

Fig. 11. Corroded microstructure (BEI) of Al + B_4C added refractory. The dense MgO layer was severely penetrated and corroded by the slag, but a thin decarburised layer and a slag penetrated layer were observed. M = MgO, V = void, G = graphite, S = slag. A: uncorroded layer; B: slag penetrated layer; C: decarburised layer; D: dense MgO layer; E: slag layer.

$$C(s) + Fe_xO(l) = xFe(g, l) + CO(g) \quad (3)$$

$$C(s) + MnO(l) = Mn(g, l) + CO(g) \quad (4)$$

Due to reactions (1)–(4), C (mainly graphite) was oxidised leaving the decarburised layer in the microstructure (Fig. 5). The large angular voids in this layer were believed to be the volumes where the original C was present, and the smaller rounded pores were most likely to be bubbles formed by the gaseous phases from reactions (1)–(4). Moreover, the presence of Fe metal with Mn in the decarburised layer (Fig. 5) verified the occurrence of reactions (3) and (4).

The precipitation of Fe metal with Mn in the decarburised layer (Fig. 5) via reactions (3) and (4) also suggested that the local atmosphere was reducing or only slightly oxidising, different from that in the slag layer. The slag layer also contained some rounded MgO grains, most likely eroded from the dense MgO layer, since they were only found in the slag close to it. The

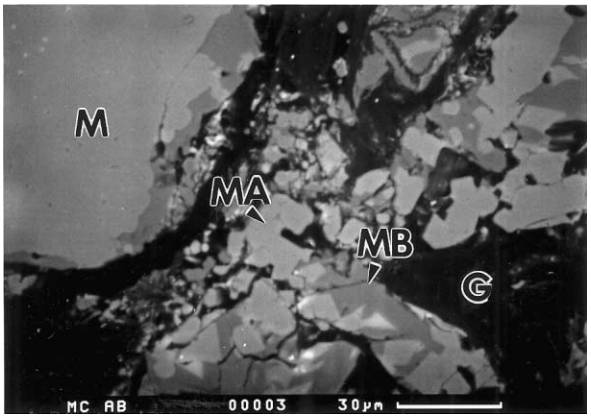

Fig. 12. High magnification BEI of the uncorroded layer shown in Fig. 11, showing that large $MgAl_2O_4$ (MA) crystals coexist with $MgO.3B_2O_3$ (MB) formed between graphite (G) in the matrix.

microstructural morphology of these MgO grains, i.e. covered with C_3MS_2 shells and with precipitation of Fe_xO and MnO inside of them, was similar to that observed in a recent study on the MgO dissolution in the same slag in air,[19] suggesting that the local atmosphere in the slag layer was strongly oxidising. The above analysis indicated that the atmosphere changed locally, becoming more oxidising with distance from the uncorroded layer to the slag layer. Because of the reducing or weakly oxidising atmosphere in the uncorroded layer, significant Mg(g) would be produced via reaction (5). As shown in Fig. 1, at 1650°C, the partial pressure of Mg(g) in the uncorroded layer (i.e. Alpha = 0) can be higher than 10^{-2} atm. Mg(g) formed from reaction (5) would diffuse towards the slag layer. When it arrived at the (original) decarburised layer/slag layer interface, because the atmosphere there was more oxidising, it would be re-oxidised back to MgO via reaction (6). The MgO so formed, and that from the decarburised layer, would dissolve into the local slag at the interface, eventually oversaturating the local slag with MgO and precipitating MgO. Precipitation of MgO from the local slag is likely responsible for the formation of slag-containing dense MgO layers (Figs. 5 and 6).

$$C(s) + MgO(s) = Mg(g) + CO(g) \quad (5)$$

$$2Mg(g) + O_2(g) = 2MgO(s) \quad (6)$$

After the formation of the dense MgO layer, the C oxidation and the MgO dissolution would be suppressed, because this layer isolated the refractory from the slag/atmosphere, although it could not stop completely the reactions. As shown in Fig. 1, MgO is not in equilibrium with the slag, so after formation of the dense MgO layer, slag could still interact with it leading to its disintegration and dissolution. Furthermore, slag which was already present in the dense MgO layer (Figs. 5 and 6) would provide additional pathways for further slag penetration and oxygen diffusion, which would lead to the corrosion of the decarburised layer and a new sequence of C oxidation and MgO dissolution. C oxidation, formation and dissolution of the dense MgO and decarburised layers maintained the corrosion processes.

4.2. Influence of additives on corrosion resistance and corroded microstructures of MgO–C refractories

As discussed above, two main sub-processes, C oxidation and MgO dissolution in the slag, were responsible for the corrosion of the basic MgO–C refractory. Therefore, the different influence of additives on the corrosion resistance of MgO–C refractories (Fig. 4) could be analysed based on their influence on these two sub-processes.

When Al was added, reactions (7)–(9) occurred in the refractory.[20] Accompanying the formation of MA via reactions (8) and (9) (Fig. 8), CO(g) was reduced back to C. Furthermore, because Al is a stronger reducing-agent than C, it would, instead of C, reduce Fe_xO and MnO from the slag to the corresponding metals [reactions (10) and (11)], as a result, reactions (3) and (4) would be inhibited. Because of these reactions, C oxidation would be (thermodynamically) inhibited. As shown in Fig. 2, with addition of Al, Alpha corresponding to the C disappearance, increases from ~2.2 (in the case of the additive-free refractory) to ~3.2. Nevertheless, comparison of the microstructure shown in Fig. 7 with that in Fig. 5 revealed that the decarburised layer in the Al added refractory was only slightly thinner than that in the additive-free refractory, suggesting that Al addition inhibited the C oxidation at 1650°C only a little.

$$4Al(g, l) + 3C(s) = Al_4C_3(s) \quad (7)$$

$$2Al(g, l) + 3CO(g) + MgO(s) = MgAl_2O_4(s) + 3C(s) \quad (8)$$

$$Al_4C_3(s) + 2MgO(s) + 6CO(g) = 2MgAl_2O_4(s) + 9C(s) \quad (9)$$

$$2Al(g, l) + 3Fe_xO(l) = 3xFe(g, l) + Al_2O_3(s) \quad (10)$$

$$2Al(g, l) + 3MnO(l) = 3Mn(g, l) + Al_2O_3(s) \quad (11)$$

$$2Al(g, l) + 4MgO(s) = 3Mg(g) + MgAl_2O_4(s) \quad (12)$$

Al addition has also been reported to accelerate the formation of the dense MgO layer by forming more Mg(g) [reaction (12)], and is believed to be beneficial to the improvement of C oxidation resistance and slag resistance.[15] However, comparison between Figs. 5 and 7 revealed that the dense MgO layer in the Al added refractory was a little thinner than that in the additive-free refractory, which is considered to be related to the negative effect of the Al addition on the MgO dissolution.

According to Yamaguchi,[21] the partial pressure of Al(g) coexisting with Al_4C_3 was high ($>10^{-3}$ atm) at the test temperature. So part of the Al(g) evaporating from the Al_4C_3 [reaction (13)] in the uncorroded layer and/or the slag penetrated layer would diffuse towards the slag layer. As stated above, the atmosphere became more oxidising towards the slag layer. So when the Al(g) arrived at the decarburised, dense MgO and/or slag layers, it would be oxidised to Al_2O_3 according to reaction (14). The Al_2O_3 so formed would interact with MgO to form MA which further dissolved in the local slag. As predicted by the thermodynamic calculations (Fig. 2), a small amount of slag could dissolve the MA formed in the refractory. This also explained why no obvious MA was observed in the dense MgO layer, and slag in the dense MgO and decarburised layers was more Al_2O_3-rich.

$$Al_4C_3(s) = 4Al(g) + 3C(s) \quad (13)$$

$$4Al(g) + 3O_2(g) = 2Al_2O_3(s) \quad (14)$$

The dissolution of Al_2O_3 (MA) in the slag would increase MgO solubility in the slag,[13] As shown in Fig. 2, compared with the additive-free refractory, Alpha corresponding to the MgO disappearance decreases from ~6.0 (in the additive-free refractory) to ~5.8. The increase of MgO solubility in the slag would accelerate its dissolution, which would counteract the positive effect of Al on the dense MgO layer formation stated above. Consequently, when Al was added, the thickness of the dense MgO layer (Fig. 7) became even thinner than that of the additive-free refractory (Fig. 5), and more Al_2O_3-rich slag was present in the dense MgO layer and more MgO grains in the layer were corroded.

It was the balance between the positive influence on C oxidation inhibition and the negative influence on MgO dissolution that resulted in the slight difference in the corrosion rates between Al added and additive-free refractories (Fig. 4).

With Si as the additive, reactions (15)–(18) would occur in the refractory.[21,22] Because of reactions (16)–(18), M_2S formed in the refractory and simultaneously CO(g) was reduced back to C, inhibiting C oxidation. As shown in Fig. 3, C disappears at higher Alpha (~3.2), compared with the additive-free refractory (~2.2). Nevertheless, comparison between Figs. 9 and 5 revealed that the decarburised layer in the Si added refractory (Fig. 9) was only slightly thinner than in the additive-free refractory (Fig. 5), suggesting that Si addition only slightly improved C oxidation resistance at the test temperature.

$$Si(l) + C(s) = SiC(s) \quad (15)$$

$$2Si(l) + 2CO(g) = 2SiO(g) + 2C(s) \quad (16)$$

$$2SiC(s) + 2CO(g) = 2SiO(g) + 4C(s) \quad (17)$$

$$2MgO + SiO(g) + CO(g) = Mg_2SiO_4(s) + C(s) \quad (18)$$

The negative effect of the Si addition on the MgO dissolution was related to the formation and dissolution of SiO_2 in the slag. SiO(g) formed in the uncorroded layer and/or the penetrated layer via reactions (16) and (17) would diffuse towards the slag layer. When it arrived at the decarburised, the dense MgO and/or slag layers, because the atmosphere there was more oxidising, it would be oxidised to SiO_2 via reaction (19).

$$SiO(g) + O_2(g) = SiO_2(s) \quad (19)$$

The SiO_2 so formed would interact with MgO to form M_2S which further dissolved in the local slag. As predicted by the thermodynamic calculations, a small amount of slag could dissolve the M_2S formed in the refractory. This also explained why no obvious M_2S was found in the dense MgO layer. The dissolution of SiO_2 (M_2S) in the local slag would decrease the slag basicity (CaO/SiO_2 ratio) and thus increase MgO solubility in the slag.[13] As shown in Fig. 3, MgO disappears at a lower Alpha (~5.6), compared to that of the additive-free refractory (~6.0). Consequently, MgO dissolution in the slag was greatly accelerated and thus a much thinner dense MgO layer was found, and more slag penetrated the dense MgO and decarburised layers (Fig. 9). The slight influence on C oxidation inhibition but a greater increase in the MgO dissolution resulted in severe corrosion in this case (Fig. 4).

Thermodynamic calculations (Fig. 3) show that the Alpha values corresponding to the disappearance of C and MgO in both additions of Al + Si and Si are almost identical, suggesting that thermodynamically both have a similar effect on the corrosion of MgO–C refractories. The macrostructure with Al + Si was similar to that with just Si addition, although a little thicker dense MgO layer was observed. The reason for this is not clear, although it may be because the presence of Al partially inhibited the oxidation processes of Si and/or SiC,[23] and thus to some extent prolonged the SiO_2 formation and

dissolution in the slag. After 30 h at 1650°C, many SiC crystals still remained in the uncorroded layer, which seems to support this deduction. The slightly different thicknesses of the dense MgO layers were probably responsible for the small difference in the corrosion rates (Fig. 4).

The main reactions occurring in the B_4C added refractory are listed below [reactions (20)–(25)].[24] Similar to the Al or Si additions, reduction of CO back to C via reactions (20)–(24) would contribute to C oxidation inhibition (Fig. 3). Furthermore, the M_3B (with melting point ~1350°C) liquid formed in the refractory [reaction (25)] would fill the pores between C and cover the C surface thus also contributing to C oxidation inhibition.

$$B_4C(s) + 6CO(g) = 2B_2O_3(g, l) + 7C(s) \quad (20)$$

$$B_4C(s) + 4CO(g) = 2B_2O_2(g) + 5C(s) \quad (21)$$

$$B_4C(s) + 4CO(g) = 4BO(g) + 5C(s) \quad (22)$$

$$B_2O_2(g) + CO(g) = B_2O_3(g, l) + C(s) \quad (23)$$

$$2BO(g) + CO(g) = B_2O_3(g, l) + C(s) \quad (24)$$

$$B_2O_3(g, l) + 3MgO(s) = 3MgO.B_2O_3(l) \quad (25)$$

Nevertheless, addition of B_4C negatively impacts on MgO dissolution. According to Yamaguchi,[24] partial pressures of BO(g), B_2O_2(g) and B_2O_3(g) at 1650°C are high ($>10^{-4}$ atm), so significant amounts of these gaseous phases would form in the refractory. They not only react with CO(g) and MgO to form M_3B liquid in the refractory, but also diffuse towards the slag layer. When these gases arrive at the decarburised, dense MgO and/or slag layers they react with MgO to form low melting phases such as M_3B which would dissolve quickly in the local slag. Furthermore, the increase in the slag B_2O_3 content would further increase MgO solubility (Fig. 3) and thus further accelerate MgO dissolution. No obvious decarburised and dense MgO layers were found between the uncorroded refractory and slag layers (Fig. 10), indicating that after they were formed they dissolved quickly into the slag. After MgO quickly dissolved in the slag, graphite in the matrix, even though well protected from oxidation, will be washed away easily by the slag, because it is held together mainly by the liquid M_3B, explaining why the addition of B_4C resulted in the worst corrosion (Fig. 4).

Differently from the other additions, addition of Al + B_4C improved markedly the corrosion resistance (Fig. 4). The reasons for this behaviour will now be discussed. Because Al and B_4C were both added, C oxidation could be inhibited via the following. Firstly, CO(g) was reduced back to C by Al and/or B_4C via e.g. reactions (8),(9), and (20). Secondly, Fe_xO and MnO from the slag were reduced via e.g. reactions (10) and (11), and thirdly M_3B liquid formed in the refractory via e.g. reaction (25), filled the pores between C (mainly graphite) and covered the C surfaces (Fig. 12). The thinnest decarburised layer formed in the microstructure (Fig. 11) indicated that C oxidation was inhibited most effectively in this case. Another notable microstructural feature was that many MA crystals [larger than those in the Al added refractory (Fig. 8)] were found between the graphite flakes in the matrix (Fig. 12). These larger MA crystals often coexisted with M_3B phases, suggesting that at the test temperature M_3B liquid might have played a role in their formation and growth. As reported by Suguru,[25] boron-containing liquid has a strong mineralising effect on MA crystallisation. This fact further indicates that graphite in the matrix which was protected from oxidation was also bonded together by MA crystals at the test temperature. Now, the negative effect of this addition on the MgO dissolution should be discussed. Similar to the Al or B_4C single additions, addition of Al + B_4C would also accelerate MgO dissolution by increasing the local slag Al_2O_3 and/or B_2O_3 contents. The mechanisms were just the combination of those in the Al addition and B_4C addition, so they are not described further here. This was reflected both in the thermodynamic calculations (Fig. 3) and microstructure (Fig. 10). As shown in Fig. 3, with this addition, Alpha corresponding to the MgO disappearance decreases from ~6.0 (in the additive-free refractory) to ~5.4, and Fig. 10 shows that a thin and more severely corroded MgO dense layer was observed. Nevertheless, the fact that the thickness of dense MgO layer (Fig. 11) was similar to that of Al + Si or Si additions, suggested that the MgO dissolution in this case was only intermediately accelerated. The reason might be similar to that of the Al + Si addition, i.e., the presence of Al partially inhibited the B_4C oxidation process [reactions (20)–(22)],[26] and thus to some extent prolonged the formation and dissolution of B_2O_3 in the slag. Based on the above analysis, the synergistic effect of addition of Al + B_4C on the corrosion resistance (Fig. 4) could be summarised as follows. B_2O_3 formed from reactions (20)–(24) reacted with MgO to form B-containing liquid [reaction (25)]. This liquid not only inhibited effectively C oxidation, but also accelerated formation and growth of MA crystals between the graphite flakes in the matrix. Thus, even after some MgO grains exposed to the slag were corroded, much graphite in the matrix was protected from oxidation and still bonded together by the MA crystals and so not easily washed away (eroded) by the slag. This helped to maintain the integrity of the whole texture and ameliorated corrosion resistance (Fig. 4).

5. Conclusions

The corrosion resistance of MgO–C refractories containing various antioxidants has been compared using a rotary slag test at 1650°C for 30 h. Thermodynamic calculations were performed, and corroded microstructures examined to assist understanding the corrosion processes. The main results are:

1. C oxidation and MgO dissolution in the slag were the main factors affecting corrosion of MgO–C refractories. Antioxidants influenced corrosion resistance of MgO–C refractories by affecting these two sub-processes.
2. Al addition improved the C oxidation resistance at 1650°C only a little but accelerated the MgO dissolution in the slag. The balance between these two contradictory factors determined the minor effect of Al addition on the corrosion resistance.
3. Addition of Si or Al + Si slightly improved the C oxidation but more greatly accelerated the MgO dissolution than the Al addition or no addition. Therefore, the refractory with Si or Al + Si showed worse corrosion resistance than that with Al or without additive.
4. Mg borate liquid formed in the B_4C added refractory, which, although effectively suppressing C oxidation, greatly accelerated MgO dissolution. In this case, after MgO grains quickly dissolved in the slag, graphite in the matrix, even though effectively protected from oxidation, would be washed away easily by the slag, because it was held together by Mg borate liquid. Consequently, this addition showed the worst corrosion resistance.
5. With double addition of Al + B_4C, a boron-containing liquid formed which not only inhibited effectively C oxidation, but also accelerated formation and growth of MA crystals between graphite in the matrix at the test temperature. In this case, even though MgO dissolution was accelerated to some extent, graphite in the matrix was effectively protected from oxidation and held in place by MA crystals and so was not easily eroded by the slag (as for the B_4C additions). This maintained the integrity of the refractory texture and thus inhibited further slag penetration and corrosion, so that refractory with this addition showed the best corrosion resistance.

Acknowledgements

We would like to thank the EPSRC (Research Grant GR/L31647), Baker Refractories (UK), Vesuvius KSR and British Steel (now Corus) for financial and in-kind support.

References

1. Taffin, C. and Poirier, J., The reaction of metal additives in MgO–C and Al_2O_3–C refractories. *Interceram*, 1994, **43**, 454–460.
2. Brant, P. O. R. C., Limm, W. A. and Grocener, C. A., Development of high erosion and corrosion resistant MgO–C bricks for BOF application. In *UNITECR'93 Proceedings, ALAFAR, Sao Paulo, Brazil*, 1993, pp. 462–71.
3. Lubaba, N. G., Rand, B. and Brett, N. H., Microstructure and strength of MgO–carbon composite refractory materials. *Trans. Br. Ceram. Soc.*, 1989, **89**, 47–54.
4. Hayashi, S., Takanaga, S., Takahashi, H. and Watanabe, A., Behaviour of boric compounds added in MgO–C bricks. *Taikabutsu Overseas*, 1991, **11**, 12–19.
5. Hanagiri, S., Harada, T. and Fugihara, S., Effects of the addition of metal and CaB_6 to magnesia carbon bricks for converters. *Taikabutsu Overseas*, 1993, **13**, 20–27.
6. Naruse, Y., Fujimoto, S., Kamata, Y. and Abe, M., Results of investigation of mag-carbon bricks used in converter. *Taikabutsu*, 1983, **3**(2), 3–7.
7. Nagai, B., Matsumura, T., Hosogawa, K. and Geji, M., Magnesia carbon bricks for hot steel ladles. *Taikabutsu*, 1986, **38**(3), 207–209.
8. Naefe, H., Seager, M. and Stusser, D., The influence of carbon carriers and antioxidants on the service life of magnesia bricks for the oxygen steel converter. *Interceram.*, (special issue) 1985, 37–40.
9. Morimoto, T., Harita, A., Imaiida, Y., Uchimura, R. and Kumagai, M., Influence of carbon purity on wear of MgO–C brick. *Taikabutsu*, 1982, **34**(6), 336–341.
10. Baker, B. H. and Brezny, B., Dense zone formation in magnesia-graphite refractories. *UNITECR'93*, 1993, 241–247.
11. Ishii, H., Tsuchiya, I., Oguchi, Y., Kawakami, T. and Takahashi, H., Behaviour of impurities in magnesia-carbon brick at high temperatures. *Taikabutsu Overseas*, 1990, **10**(1), 3–8.
12. Uchimura, R., Kumagai, M., Ohishi, I., Ogusahara, K. and Morimoto, T., Development of high performance magnesia-carbon bricks for BOF. *Interceram.*, (special issue) 1985, 63–66.
13. Zhang, S. and Lee, W. E., Use of phase diagrams in the study of refractories corrosion. *Int. Mater. Rev.*, 2000, **45**(2), 41–58.
14. Watanabe, A., Matsuki, T., Takahashi, H. and Takahashi, M., Effects of metallic elements addition on the properties of magnesia-carbon bricks. In *Proc. of 1st Int. Conf. Ref., Tokyo*, 1983, pp. 125–134.
15. Li, X. and Rigaud, M., Oxidation and corrosion resistance of MgO–C refractories with antioxidants, In *'96 Int. Symp. Ref.; Haikou, China,* International Academic Publishers, November 1996, pp. 514–520.
16. Zhang, S., Rezaie, H. R., Sarpoolaky, H. and Lee, W. E., Al_2O_3 dissolution into silicate slag. *J. Am. Ceram. Soc.*, 2000, **83**(4), 897–903.
17. Lee, W. E. and Zhang, S., Melt corrosion of oxide and oxide–carbon refractories. *Int. Mater. Rev.*, 1999, **44**(3), 77–104.
18. Goto, K., Argent, B. B. and Lee, W. E., Corrosion of MgO–$MgAl_2O_4$ spinel refractory bricks by calcium aluminosilicate slag. *J. Am. Ceram. Soc.*, 1997, **80**(2), 461–471.
19. Zhang, S., Sarpoolaky, H., Marriott, N. and Lee, W. E., Penetration and corrosion of magnesia grain by silicate slags. *Trans. Br. Ceram. Soc.*, 2000, **99**(6) 248–255.
20. Brant, P. O. R. C. and Rand, B., Reactions of silicon and aluminium in MgO–graphite composites: (Part 1) effects on porosity and microstructure. *UNITECR'93*, pp. 247–250.
21. Yamaguchi, A., Behavior of SiC and Al added to carbon-containing refractories. *Taikabutsu Overseas*, 1984, **4**(3), 14–18.
22. Zhang, S., Marriott, N. and Lee, W. E., Thermochemistry and microstructures of MgO–C refractories containing various antioxidants. *J. Eur. Ceram. Soc*, 2001, **21**(8), 1037–1047.

23. Yamaguchi, A., Behavior of boron carbide added to carbon-containing refractories. *Taikabutsu*, 1983, **36**(10), 558–563.
24. Yamaguchi, A. and Tanaka, H., Role and behaviour of non-oxide compounds added to carbon-containing refractories. *UNITECR'93 Proceedings*, 1993, pp. 32–38.
25. Surugu, T., Effect of Mg–B material addition to MgO–C bricks. *Taikabutsu*, 1994, **46**(5), 269–276.
26. Zhang, S., Yamaguchi, A. and Hashimoto, S., Behavior of anti-oxidants added to carbon-containing refractories. *UNITECR'95, Kyoto, Japan,* 1995, pp. 341–348.